Available online at www.sciencedirect.com
SCIENCE DIRECT
Polymer 46 (2005) 12468–12479
polymer
www.elsevier.com/locate/polymer

Nanostructured polymer blends: Synthesis and structure

Todd M. Alam [b], Joshua U. Otaigbe [a,*], Dave Rhoades [a], Gregory P. Holland [b], Brian R. Cherry [b,1], Paul G. Kotula [b]

[a] School of Polymers and High Performance Materials, University of Southern Mississippi, 118 College Drive #10076, Hattiesburg, MS 39406-0076, USA
[b] Sandia National Laboratories, Department of Electronic and Nanostructured Materials, Albuquerque, NM 87185-0886, USA

Received 18 July 2005; received in revised form 15 October 2005; accepted 17 October 2005
Available online 4 November 2005

Abstract

Nanostructured polymer blends prepared via anionic ring opening polymerizations of cyclic monomers in the presence of a pre-made polymer melt exhibit a number of special properties over traditional polymer blends and homopolymers. Here, we report on a simple and versatile method of in situ polymerization of macrocyclic carbonates in the presence of a maleic anhydride polypropylene (*m*PP) matrix and a surface-active compatibilizer (i.e. PC grafted onto a *m*PP backbone generated in situ) to yield a micro- and nanostructured polymer blends consisting of a polycarbonate (PC) minor phase, and a polypropylene (PP) major phase. By varying the processing conditions and concentration of the macrocyclic carbonate it was possible to reduce the size of the PC dispersions to an average minor diameter of 150 nm. NMR and TEM characterizations indicate that the PC dispersions do not influence crystal content in the PP phase. Overall, the results point to a simple strategy and versatile route to new polymeric materials with enhanced benefits.

Keywords: Nanostructured polymer blends; Morphology and dynamics; In situ polymerization

1. Introduction

Blending of polymers is one of the most important methods used to obtain new polymeric materials. Over 30% of commercial polymers used worldwide are polymer blends or alloys in one form or another [1]. One significant example of a polymer blend is acrylonitrile butadiene styrene resin which is a blend of three polymers: polybutadiene, styrene–acrylonitrile copolymer and polybutadiene grafted styrene-acrylonitrile copolymer [1,2]. The large-scale global utilization of polymer blends is primarily due to the fact that two or more polymers with vastly different properties can be melt-blended to give a new material having a synergistic combination of properties that surpasses those of the individual polymer components. The morphology evolution during polymer melt blending is a complex and interesting phenomenon that is poorly understood and has been the subject of intense study by various researchers [1,3,4]. But the ability to predict the morphological evolution of a polymer blend remains an elusive goal. It is believed that the criteria for formation of a homogeneous polymer blend such as rubber-modified plastics [1,2] is governed by a phase inversion process that is strongly affected by factors such as polymer droplet break-up and coalescence, viscosity ratio, type of mixer, melting characteristics, and the addition procedure of the components of the polymer blend. Recently, Moldenaers and co-workers [5] reported the effect of block copolymer architecture on the suppression of droplet coalescence and on the interfacial elasticity in immiscible blends of polydimethylsiloxane and polyisoprene with a droplet/matrix morphology. They showed that suppression of coalescence is more effective when the amount and overall molecular weight of the block copolymer compatibilizer increases.

There are two possible routes to generating polymer blends. The first and most common route is physical blending (without chemical reaction), such as melt- or solvent-blending of polymers [1,3]. In this method preserving the morphology during melt blending is unfeasible with mechanical mixing alone due to the strong thermodynamic tendency of the material to move towards the equilibrium phase-separated (two layers) morphology once the mixing is stopped. The second method is a chemical blending of reactive components to afford a molecularly-mixed polymer blend or copolymer [6–8]. In the chemical blending method, prescribed chemical reactions (e.g.

* Corresponding author. Tel.: +1 601 266 5596.
E-mail address: joshua.otaigbe@usm.edu (J.U. Otaigbe).
[1] Present address: Bruker Biospin, Inc., Billerica MA.

0032-3861/$ - see front matter © 2005 Elsevier Ltd. All rights reserved.
doi:10.1016/j.polymer.2005.10.079

graft or block copolymerization reactions) take place during the blending process. The most common monomer used in the chemical blending method is maleic anhydride or its analogs such as citaconic and fumaric acids. The facile physical blending method although limited is well developed while, the chemical blending method is much more complicated and less studied [9,10]. Besides the work of White and co-workers [11,12], there is very little reported effort to quantitatively understand the reactive extrusion or graft copolymerization in extruders.

Presently, there is great interest in micro- and nano-length scale technologies in which polymer blends could play an important role, but the physics and technology of processing polymeric blends when the size of the dispersed (minor) phase is comparable to the sample dimension is not well understood [13]. As already mentioned the size and morphology of the dispersed component is determined during polymer processing and is crucial to the final physical properties. Because the chemical blending method is relatively new and offers a number of exciting possibilities for the future, the present article will explore its feasibility in generating nanostructured polymer blends that contain a stable, molecularly dispersed phase having length scales ranging from 10 to 100 nm. Like others have reported for a different polymer blend system [14], it will be shown that the strategy adopted in our study is feasible via the rational selection of appropriate starting materials, processing conditions (such as temperature, shear rates (rpm), residence time, relative composition of blend components, and stoichiometry of reactants), and of a prescribed in situ chemical reaction. By obtaining detailed information regarding the composition-processing-property behavior of the nanoblend polymers reported here, it may reduce or eliminate costly 'trial and error' practice that is common in the literature and industry. The expected unique and interesting properties of the nanostructured blends include: (1) thermodynamically stable, melt-processable polymer blends structured on submicrometer length scales; (2) relatively low cost method to preserve the optimized morphology during processing facilitated by compatibilizing agents formed in situ; (3) potential to improve material transparency, creep and solvent resistance; (4) potential to simultaneously increase tensile strength and ductility or energy to break; and (5) favorable rheological properties in comparison to physical blends with compatibilizers. These properties should open new applications hitherto inaccessible to pure polymers and their physical blends or composites.

In this article, we explore the feasibility of one-step, reactive extrusion [15] of reactive components based on the fast anionic ring-opening polymerization (ROP) of cyclic aromatic carbonate monomers [16,17] in a matrix of a commercial polymer such as polypropylene to afford a nanostructured polymer blend with unique and interesting properties. The advantages of using anionic ROP are fast kinetics, high monomer conversion, no side product, low viscosity of the oligomeric mixtures, and elimination of highly corrosive chemicals such as phosgene from the polymer processing equipment [18]. The resulting nanostructured polymer blend is expected to contain a unique structure, where one polymer is dispersed within another continuous polymer phase at molecular length scales that are impossible to achieve via classical polymer blending. In addition, the paper will investigate use of a chemical compatibilizer or an in situ chemical reaction that can reduce interfacial tension between the components of the polymer blend to allow generation of large aggregates of the nano-dispersed phase by preventing these particles from coalescing in the continuous polymer phase. Furthermore, the paper utilizes NMR and TEM characterization techniques to probe the underlying morphological, structural and chemical processes involved in the nanoscale materials and observed phenomena. The morphology of the nanostructured polymer blends is observed to be remarkably stable even at elevated temperatures and the crystallization kinetics of the blend were found to be unexpectedly accelerated by the presence of the nanostructured dispersed component [19].

One motivation for our long-range research program is to discover a facile, inexpensive route to nanostructured polymer blends as well as to determine correlations between the synthesis and processing conditions and the microscopic and macroscopic properties of these new nanostructured polymer blend systems. In addition, the potential to combine, in a single material, two immiscible polymer components at the nanometer length scale is thought to represent an exciting possibility with extraordinary implications for the rational design of novel multifunctional materials having a wide range of tailored structures and properties. The present study may stimulate a better understanding of the rational design of stable nanostructures in polymer blends that were previously unfeasible for classical polymer blends, making the strategy useful and widely applicable. The potential versatility of the nanostructured polymer blends will make them useful in a variety of high performance applications such as optics, drug delivery, tissue engineering and permeable membranes for separation technology.

2. In situ polymerization, compatibilization and blending strategy

As described in a review article by Otaigbe [20], researchers at General Electric Corporate Research have established the versatility of pseudo-high dilution, triethyl amine-catalyzed hydrolysis and condensation of bisphenol A (BPA)-bischloroformate (BCF) to form oligomeric cyclic carbonates that can be made to undergo ROP in a separate reaction [21–26]. The ROP reaction is unique because it is driven almost entirely by entropy; the reaction is nearly thermo-neutral, with an enthalpy change of less than -1.25 kJ/mol and a calculated entropy change of about 55 kJ/mol K [21–23,25]. A typical production scheme involves conversion of BPA into its BCF, then reaction under standard cyclization conditions to produce cyclic oligomeric carbonates. The latter is converted to pure high molecular weight polymer (weight-average molecular weight

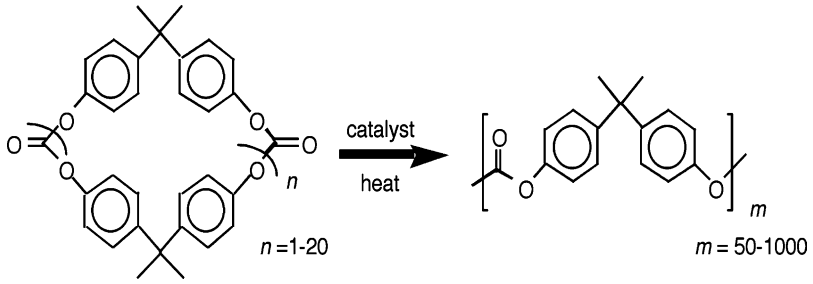

Scheme 1. Ring-opening polymerization of cyclic aromatic carbonates to form polycarbonate [Adapted from Refs. [20,24–26]].

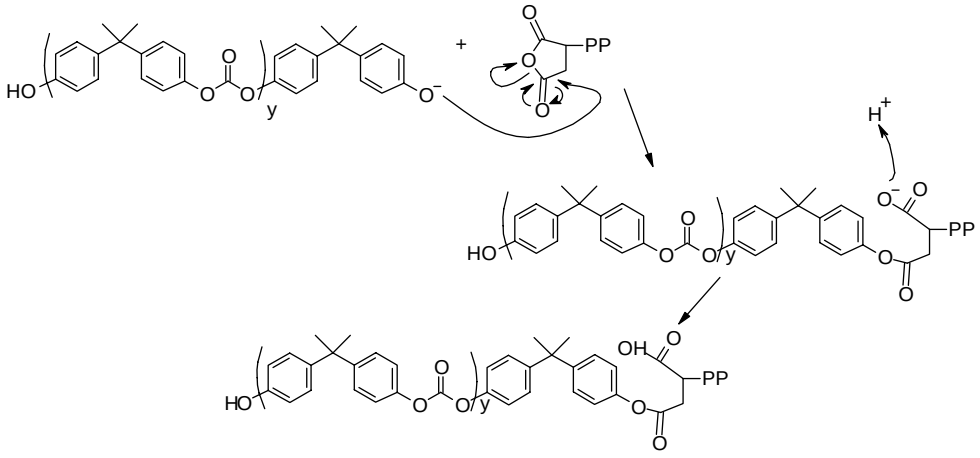

Scheme 2. A growing polycarbonate chain chemically grafts onto the maleic anhydride functional group on the polypropylene chain.

=200,000–400,000) [21–23,25][2] by heating it in the presence of an initiator (reaction Scheme 1). Highly effective catalysts such as tetrabutylammoniumtetraphenylborate can be used to drive the ROP of the cyclic carbonates to completion thus leading to polycarbonates with polydispersities of about 2 [24,26]. The overall reaction mechanism and additional details are reported in the literature [20–23,26].

A variety of functional groups including ester, amide, sulfone, urethane and ether can be incorporated into the above cyclic aromatic carbonates (from BCF or cyclic oligomers) to produce a wide variety of very high molecular weight polymers relative to conventionally prepared polycarbonates [27–29]. Furthermore, copolymers can be readily prepared by reacting the 'living' hydroxy-terminated linear polycarbonates with other monomers or reactive polymers (e.g. cyclic siloxanes or chlorosilane-terminated polydimethylsiloxane) [27,28].

Thus, the ROP of the above species within a suitable polymer melt or cyclic oligomer [30] has the potential to produce high molecular weight, nanostructured polyaromatic carbonates or their copolymers with novel structures and functional properties for beneficial uses in a number of applications. Use of the oligomeric cyclic aromatic carbonates eliminates from the polymer processing equipment the highly corrosive phosgene in addition to the other benefits of ROP already discussed.

In this study, in situ ROP of cyclic aromatic carbonates was used to yield the minor phase and graft copolymer compatibilizers [31,32]. The in situ polymerization and compatibilization is characterized by fast reaction kinetics, high monomer conversion, no side reactions, and low viscosity of oligomeric materials as already mentioned [32]. Specifically, fast anionic ROP reaction kinetics occur on a time scale such that the minor phase interface is sufficiently covered with compatibilizer during surface generation; this greatly reduces the chance of the graft compatibilizer forming micelles [31]. Instead of the softened/melted droplet being required to break apart under shearing and mixing forces, reactive compatibilization via in situ polymerization creates a polymer droplet already sufficiently covered with surface-active compatibilizer [31,33].

The thermodynamic stability of the nanostructured polymer blend is increased to such a degree that high surface area nanostructured droplets are stable even after shearing is stopped and with thermal fluctuations [32]. This synthesis method provides an efficient and economical method to generate nanostructured immiscible polymer blends by completing the conversion of raw materials into final products in one reaction extrusion step, thus eliminating the cost associated with functionalizing the polymers prior to reactive blending. Because traditional processing equipment such as extruders can be used, the process set up time is faster, reducing start up costs and lowering the costs of production. Using a counter-rotating twin-screw extruder described later, the

[2] Conventionally prepared polycarbonates have weight-average molecular weight in the range of 40,000–60,000.

macrocylic carbonate was anionically polymerized in situ in the presence of maleic anhydride modified polypropylene. It is hypothesized that during the in situ polymerization some of the growing chain ends react with the maleic anhydride functional group on the polypropylene generating a PP-*g*-PC graft copolymer as shown in reaction Scheme 2.

This graft copolymer effectively reduces the surface tension between the two polymer domains, allowing a larger surface area relative to the smaller volume ratio between the blends. It is noteworthy that the viscosity ratios of the in situ polymerized and compatibilized polymer blends are much closer to unity due to the relatively low viscosity of the macrocyclic carbonate at the reactive blending processing temperature used [19]. The counter-rotating twin-screws provide shear heating that rapidly melts the PP and initiates the PC polymerization process that continues throughout the length of the screw flights. The morphology of the in situ polymerized polymer blend is tuned by changing the reaction conditions as will be demonstrated later. A fraction of the reactions in the extruder will involve the ROP of oligomeric cyclic aromatic carbonates using catalytic amounts of tetrabutylammoniumtetraphenylborate and heat according to reaction Scheme 1. Because of polycarbonate's sensitivity toward free amines, adequate precautions were taken to remove any free amine from the reaction system. The specific conditions used for synthesizing the nanostructured polymer blends of this study are described in the next section.

3. Experimental section

3.1. Materials preparation

In situ polymerized and compatibilized polypropylene/polycarbonate (PP/PC) blends were generated using two melt blending devices: a Haake Polydrive (PD) torque rheometer and a Haake Minilab (ML) counter-rotating twin-screw extruder (Rheomex CTW5). The PD torque rheometer was used to generate samples in a batch-mixing environment. Sample sizes of approximately 60 g were mixed for 10 min at 200 °C and a rotor speed of 80 rpm. Macrocyclic carbonate was mixed at volume ratios of 3, 5, 10, and 20% with maleic anhydride grafted polypropylene (*m*PP) functionalized at 0.5% by weight (Samples 1-PD to 5-PD in Table 1). The macrocyclic carbonate was synthesized at GE laboratories and the maleic anhydride grafted polypropylene was supplied by Crompton Corporation. The anionic ROP of macrocyclic carbonate was catalyzed by tetrabutylammonium tetraphenylborate (TBATPB) added at a 1% weight ratio.

The ML twin-screw extruder is different from the torque rheometer in that smaller samples sizes are generated at higher shear rates that are impossible to achieve in the torque rheometer. The material can then be directly extruded and cooled to lock in the special morphology that is facilitated by the elongational and shear flow fields in the extruder. For our studies, samples were generated at ratios of maleic anhydride grafted polypropylene to macrocyclic carbonate (*m*PP-*g*-PC) of 80:20 and 90:10 by volume. The sample nomenclature adopted here is such that the second double-digit number denotes the volume concentration of the dispersed PC phase in the *m*PP phase. The material was either directly extruded once or recycled back to the inlet of the extruder to be remixed by the twin screws. For the 80:20 ratios (Samples A-ML through H-ML in Table 1) the materials were prepared at 225 and 250 °C under direct extrusion (DE) and 3 min melt recycle-mixing times. Upon exit from the extruder die, the molten material was rapidly solidified by pressing it onto an aluminum plate that removed the heat. The 90:10 *m*PP-*g*-PC sample (Sample I-ML in Table 1) was prepared at a lower melt temperature of 200 °C and 70 rpm. These processing conditions were found to give reproducible results. In the direct extrusion, a nitrogen blanket located at the die exit was used to cool the 90:10 *m*PP-*g*-PC extrudate. The 80:20 *m*PP-*g*-PC extrudate was cooled by placing it on aluminum cooling plates. The sample preparation conditions for the different samples are summarized in Table 1.

3.2. Microscopy analysis

For transmission electron microscopy (TEM), the samples were encased in epoxy, microtomed to thicknesses <100 nm, and stained for 30 min with OsO_4. The last step provided electron scattering contrast between the PC and PP domains.

Table 1
Summary of sample preparation conditions for samples synthesized with the Minilab (ML) counter rotating extruder and PolyDrive (PD) torque rheometer

Blend	PC (%vol)	PP (%vol)	Temperature (°C)	Mix rate (rpm)	Mix time (min)
A-ML	20	80	225	70	3
B-ML	20	80	225	200	3
C-ML	20	80	225	70	0
D-ML	20	80	225	200	0
E-ML	20	80	250	200	3
F-ML	20	80	250	70	3
G-ML	20	80	250	70	0
H-ML	20	80	250	200	0
I-ML	90	10	200	70	0
1-PD	0	100	200	80	10
2-PD	3	97	200	80	10
3-PD	5	95	200	80	10
4-PD	10	90	200	80	10
5-PD	20	80	200	80	10

The samples were imaged by traditional bright-field TEM analysis as well as annular dark-field scanning transmission electron microscopy (STEM) at magnifications of 8500× and 420×, respectively, on a FEI Tecnai F30-ST operated at 300 kV. STEM imaging was preferred over the standard TEM analysis, as STEM scans the polymer sample with a focused low-current electron beam, whereas in TEM broad illumination is utilized, which was found to increase sample degradation. PC particle size measurements were obtained using ImageJ computer analysis software.

3.3. Calorimetric measurements

DSC measurements were performed on a Perkin–Elmer diamond DSC apparatus cooled with liquid nitrogen. The temperature scale was calibrated with indium. The samples were finely ground, placed in sealed aluminum pans, and scanned at a temperature rate of 10 °C for four heat/cool cycles. One heat/cool cycle is defined as heating the sample from 25 to 180 °C, holding it at 180 °C for 5 min and then cooling the sample to 25 °C. To estimate the degree of crystallinity, we used 165 J/g as the heat of fusion of 100% crystalline polypropylene [34].

3.4. NMR measurements

All solid-state ^{13}C magic angle spinning (MAS) and cross polarization (CP)-MAS NMR experiments were performed on a Bruker Avance-400 instrument operating at 100.6 and 400.2 MHz for ^{13}C and ^{1}H, respectively. Spectra were obtained using a 4 mm broadband double resonance MAS probe with sample spinning rates between 10 and 15 kHz, and 1–2 K scan averages. All ^{13}C NMR pulse sequences utilize two-pulse phase modulation (TPPM) ^{1}H decoupling, with a 15° phase shift [35]. One-dimensional direct polarization (DP) MAS ^{13}C spectra utilized a recycle delay of 400 s and a $\pi/2$ pulse of 3.8 μs. The CP-MAS experiments utilized a variable amplitude ramped 2 ms contact time, a 5 s recycle delay and a $\pi/2$ pulse of 3.25 μs. The ^{1}H dipolar-filtered ^{13}C-detected CP-MAS NMR experiments were performed using the sequence previously described [36]. All chemical shifts were referenced to the carbonyl resonance of the secondary standard glycine ($\delta = 176$ ppm with respect to TMS $\delta = 0$ ppm).

The solid-state ^{1}H MAS NMR experiments were performed on a Bruker Avance-600 instrument operating at 600.14 MHz. Spectra were obtained using a 2.5 mm double resonance probe spinning between 25 and 35 kHz, using a 3 μs $\pi/2$ pulse length, 16–64, scan averages, a 4 s recycle delay, at temperatures from 25–90 °C. The dipolar-filtered ^{1}H MAS NMR spectra were obtained using the previously described sequence [37,38], with a inter-pulse delay of 10–15 μs with between 1 and 2 multi-pulse cycles. It is known that the high rotor spinning speeds causes additional heating of the sample. From independent calibrations utilizing $PbNO_3$, it was determined that at 25 kHz spinning the sample temperature is raised ~31 °C above the set temperature. All reported samples temperatures have been corrected for this sample heating. The ^{1}H NMR chemical shifts were referenced to a secondary adamantane reference ($\delta = +1.63$ ppm) with respect to TMS ($\delta = 0.0$ ppm).

4. Results and discussion

4.1. Polymer characterization

The different nanostructured polymer blends (nanoblends) detailed in Table 1, were characterized using DSC, TEM and NMR spectroscopy, with the characterization results being summarized in Table 2. From these DSC measurements the content of crystalline polypropylene (PP) present in the sample was calculated. The direct polarization (DP) solid state ^{1}H and ^{13}C MAS NMR spectra are shown in Figs. 1 and 2, along with the corresponding spectral assignments. From the ^{13}C MAS

Table 2
Experimentally determined crystallinity, minor domain size, and equilibrium spin relaxation times for nanoblend samples

Sample ID	Percent crystallinity estimated by			TEM PC domain size (nm)		NMR (ms)[a]	PP crystal size (nm)[b]		
	DSC	^{1}H NMR	^{13}C NMR	$\langle d_{major} \rangle$ (nm)	$\langle d_{minor} \rangle$ (nm)	$\sqrt{\tau_m^*}$	$\varepsilon = 1$	$\varepsilon = 2$	$\varepsilon = 3$
A-ML	–	60±5	65±2	1900	1400	11.9	6	11	17
B-ML	–	57±5	64±2	1500	1250	11.6	6	11	17
C-ML	–	–	62±2	700	500	–	–	–	–
D-ML	–	–	59±2	1200	850	–	–	–	–
E-ML	–	60±5	59±2	1700	1500	11.4	5	11	16
F-ML	–	59±5	61±2	1700	1000	11.0	5	11	16
G-ML	–	62±5	60±2	Insufficient data [c]		11.0	5	11	16
H-ML	–	63±5	66±2	Insufficient data [c]		10.9	5	11	16
I-ML	–	–	–	210	150	7.2[d]	3[d]	7[d]	10[c]
1-PD	56±1	–	–	–	–	–	–	–	–
2-PD	–	63±5	–	–	–	–	–	–	–
3-PD	52±1	63±5	–	–	–	–	–	–	–
4-PD	58±1	61±5	–	–	–	–	–	–	–
5-PD	54±1	62±5	–	–	–	–	–	–	–

[a] Determined from the ^{1}H detected ^{1}H–^{1}H spin diffusion experiments at 90 °C.
[b] Domain sizes estimated using Eq. (1).
[c] Too few PC domains in the images for reliable statistical analysis.
[d] Determined from the ^{13}C detected ^{1}H–^{1}H spin diffusion experiments at a NMR measurement temperature of 75 °C.

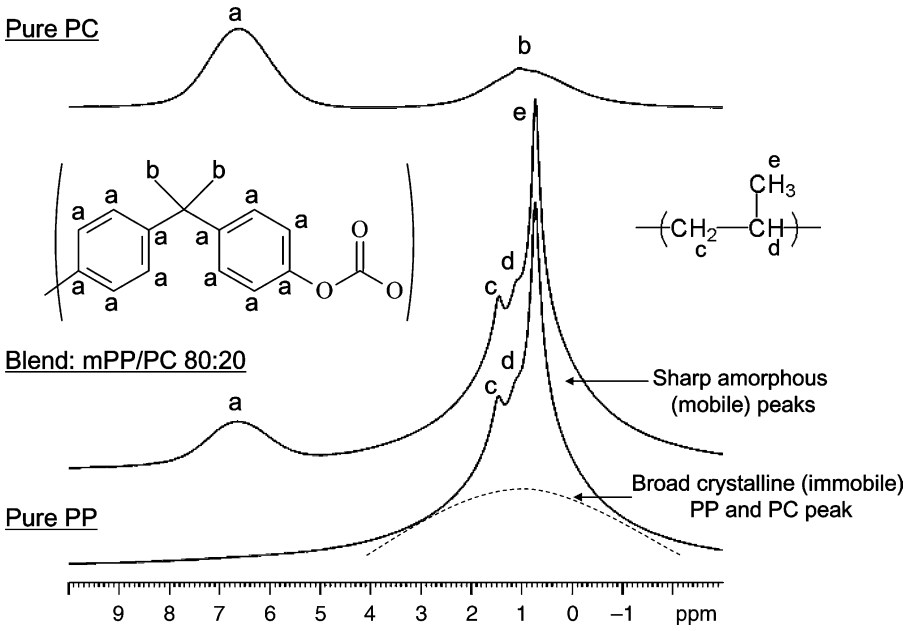

Fig. 1. ^{1}H MAS NMR of the pure PC and *m*PP and the *m*PP-*g*-PC 80:20 blend. The peak assignments of the different components are given.

NMR spectra it is clear that the polycarbonate (PC) and PP component are resolvable. The ^{13}C MAS NMR confirms that the PP is isotactic (*i*-PP) and is in the β-form, involving 3_1 helices packing with the same handedness [39,40]. High resolution solution ^{13}C NMR revealed no resonances for unreacted anhydrides or partially reacted carboxylic acid carbon species ($\delta = +170$–180 ppm) present in the final nanoblends ($\ll 1\%$ of the PP concentration) demonstrating that the grafting reaction was successful. Fig. 3(a) shows the temperature variation of the DP ^{13}C MAS NMR of pure PP as a function of the measurement temperature. Resonances for both the amorphous and crystalline PP are observed as previously described [41]. Similar temperature variations in the ^{13}C MAS NMR were observed for all the nanoblend samples. The intensity of the amorphous PP resonance increases with higher temperatures, but becomes constant above $\sim 70\,^{\circ}$C, thus allowing a measurement of PP crystallinity by direct spectral integration at elevated temperatures. The degree of PP crystallinity was also estimated from both the ^{1}H MAS NMR

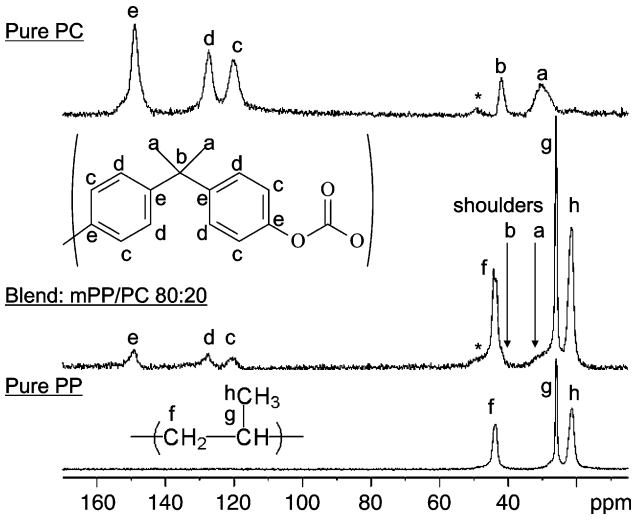

Fig. 2. The DP ^{13}C MAS NMR of the pure PC and *m*PP and the *m*PP-*g*-PC 80:20 blend. These peak assignments of the different components are given. Spinning sidebands are denoted by *.

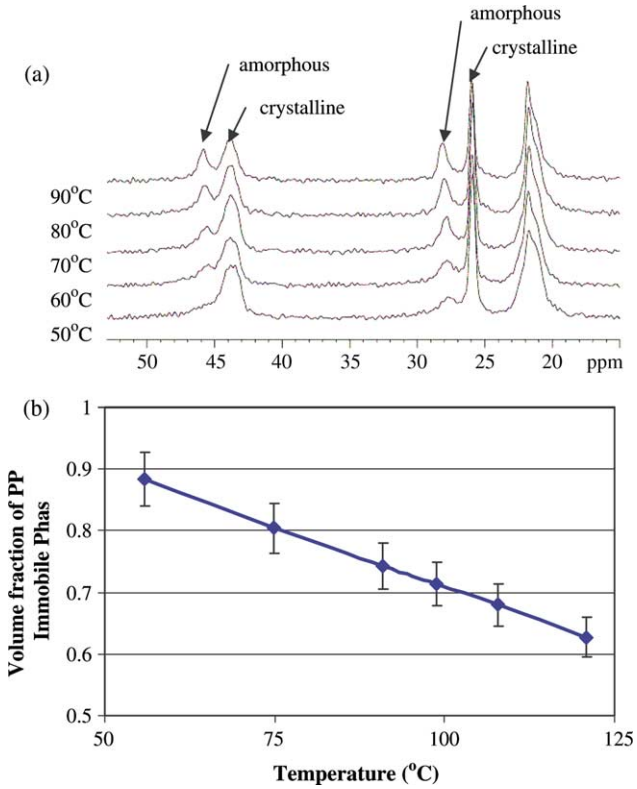

Fig. 3. The (a) DP ^{13}C MAS NMR spectra of pure PP as a function of measurement temperature. The amorphous and crystalline resonances are identified. The (b) volume fraction of the PP immobile (crystalline) phase as a function of NMR measurement temperature for the 97:03 *m*PP-*g*-PC nanoblend as measured by ^{1}H MAS NMR.

results by deconvolution of the narrow and broad spectral components (see additional discussion below). The percent PP crystallinity measured by ^{13}C and ^{1}H MAS NMR are given in Table 2. The large error bars associated with the ^{1}H MAS NMR estimate stems from the spectral overlap of the immobile (on the sub-ms time scale) and mobile component, and the strong temperature variation (see discussion below). In general, there was very little variation of PP crystallinity with processing conditions. The crystallinity estimated from ^{1}H and ^{13}C NMR spectra were typically slightly higher than the DSC results, but part of this results from the impact of temperature on the local chain mobility (see discussion below). Nevertheless the NMR results are consistent with the DSC findings in that no major variations in crystallinity were observed with processing conditions for these *m*PP-*g*-PC nanoblends.

It is worth noting that instead of referring to the PP phases observed via ^{1}H NMR as crystalline and amorphous, it is more proper to refer to the different PP phases as immobile and mobile on the sub ms time scale. This distinction between crystallinity and mobility arises since the ^{1}H MAS NMR line shape differences are dominated by changes in line width (not chemical shift), and are, therefore, a result of polymer dynamics. It is generally argued that the crystalline PP phase is immobile (on the sub-ms time scale) and gives rise to the broader (larger dipolar coupling) resonance. The motional averaging (faster than the ms timescale) within the mobile PP phase partially reduces the homonuclear ^{1}H–^{1}H dipolar coupling giving rise to the narrow line shape. The amorphous PP can give rise to both mobile (narrow) and immobile (broad) signals depending on the extent of motional averaging. The distinction between these two PP phases is now a function of the residual dipolar coupling (i.e. the NMR time scale of local motions). Assuming that the crystallites do not change size at temperatures well below the melting point (i.e. the crystalline/amorphous boundary remains constant), the immobile/-mobile ^{1}H boundary distinction (or gradient) is therefore expected to change with temperature as shown in Fig. 3(b) for the 97:03 nanoblend. The concentration of the mobile phase increases linearly with increasing temperature allowing for the determination of the mobile/immobile phase ratio at any temperature. Eventually at sufficiently elevated NMR measurement temperatures (~130–135 °C) the percent rigid phase equals the percent crystallinity of 60%, as estimated by DSC. In the case of the ^{13}C MAS NMR results, it is not averaging of the ^{1}H–^{1}H homonuclear dipolar coupling (as in the case of the ^{1}H MAS NMR), but averaging of the ^{13}C chemical shift distribution that produces the spectral change seen in Fig. 3(a). These results demonstrate that care must be exercised in comparing ^{1}H and ^{13}C MAS NMR spectra for determination of crystallinity.

4.2. PC morphology

In the nanoblends investigated, the PC phase separates from the PP phase during mixing due to the chemical incompatibility of the polymer molecules. This phase separation is clearly visible in the TEM images of these materials, as seen for the

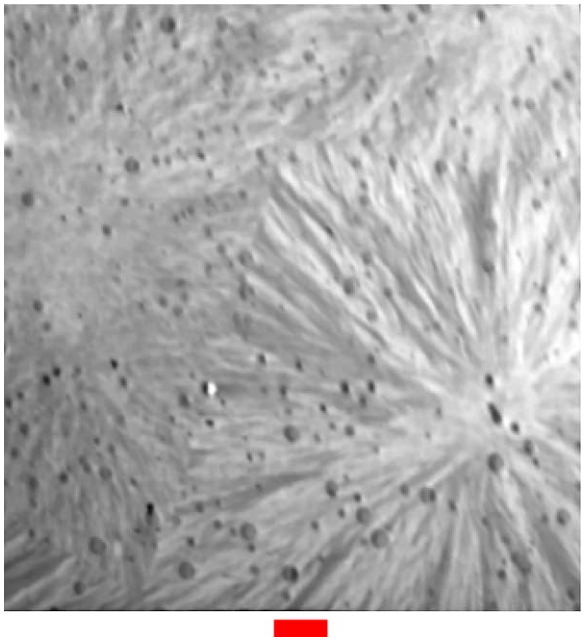

Fig. 4. TEM image of *m*PP-*g*-PC 80:20 blend (scale bar equals 2.5 μm).

*m*PP-*g*-PC 80:20 sample in Fig. 4. In the TEM images the PC phase is stained black, forming small elliptical dispersions encased within a PP matrix. Changing the processing conditions alters the size of the polycarbonate domains. The average PC domain size for the different nanoblend samples is given in Table 2.

The effects of a number of processing parameters including temperature, mixing rate and residence time on the PC morphology was investigated. As previously mentioned the twin-screw extruder used for the synthesis of the in situ compatabilized blends provides a high shear environment and has two mixing methods. The material was either directly extruded (mix time = 0) or cycled back to the inlet of the extruder to be remixed by the twin screws (mix time = 3 min or greater). When the melt was directly extruded (mix time = 0) from the barrel with a mixing rate of 70 rpm the polycarbonate domains had average elliptical dimensions of 700 by 500 nm for an *m*PP-*g*-PC melt-mixed at 225 °C. This domain size increased slightly to 1200 by 850 nm with increased mixing rate (200 rpm). Yet when the melt is set to cycle and remixed, the average droplet diameters increased dramatically to 1900 by 1400 nm at 70 rpm, but only to 1500 by 1250 nm for 200 rpm. These variations in the PC morphology with mixing time are readily seen in Fig. 5 where the PC dispersions are much larger when the material is cycled as compared to direct extrusion. The change in processing temperature (225–250 °C) had minimal impact on the results. We propose that the observed increased size of the polycarbonate dispersions is ascribed to increasing molecular weight of the growing polymer chains and droplet coalescence that occurs in the recycle loop which has a relatively lower shear environment. Thus, once the droplets reach a sufficient size and the polymer reaches a sufficient molecular weight, the size of the dispersions can no longer be reduced by re-shear in the twin-

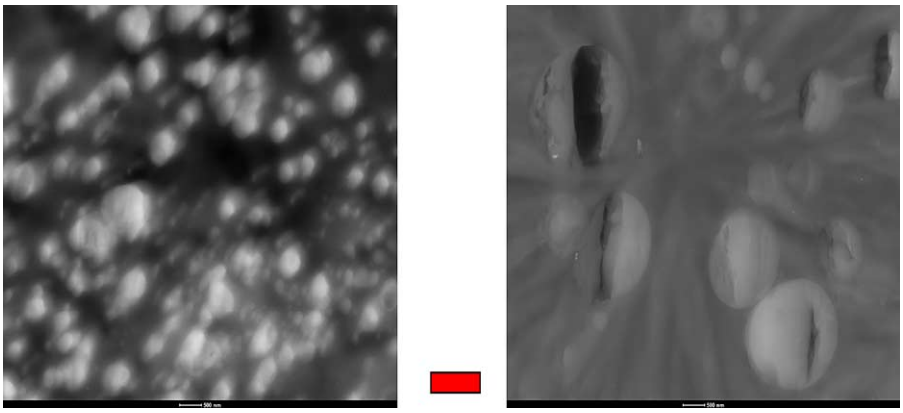

Fig. 5. STEM images of *m*PP-*g*-PC 80:20 blends prepared (left) 225 °C directly extruded and (right) 250 °C melt cycled for 3 min. The average PC dispersion size is (left) 700×500 nm^2 and (right) 1900×1400 nm^2. Scale bar equals 1 μm.

screws of the extruder. These results clearly demonstrate that variations in processing can directly impact the micro- and nanoblend morphology. NMR spin-diffusion experiments were also investigated as a possible means to measure PC morphology, but the large PC domain sizes (>500 nm) preclude the use of these types of NMR experiments due to relaxation effects.

By changing the nanoblend composition and reducing the processing temperature it is feasible to reduce the PC dimensions. Fig. 6 shows the STEM of a 90:10 *m*PP-*g*-PC nanoblend, which has an average PC domain size of 210×150 nm (Sampe I-ML in Table 2). For the processing of this blend composition, the temperature was reduced to 200 °C, the lowest possible temperature possible for the TBATPB catalyst to still be effective. The second processing change is a nitrogen air blanket was used to cool the extruded material. It is hypothesized that the low reaction temperature prevents the particles from coalescing while polymerization is taking place during shearing in the extruder. This in combination with the rapid cooling of the nanoblend prevents the polycarbonate dispersions from coalescing after extrusion.

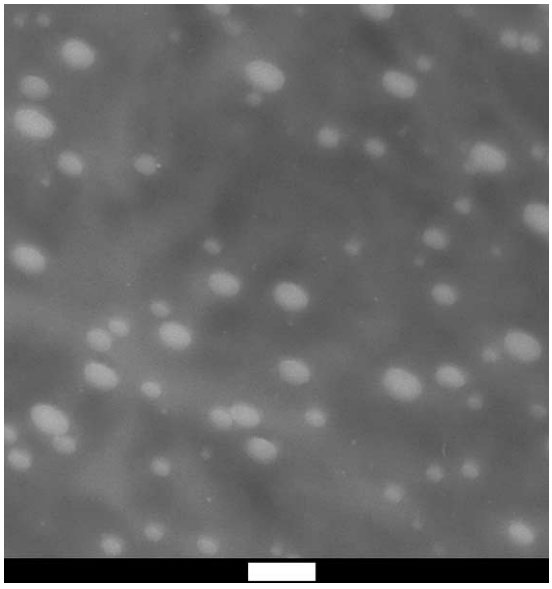

Fig. 6. STEM image of a 90:10 *m*PP-*g*-PC blend where the average PC dimensions were 210 nm×150 nm. Scale bar equals 500 nm.

4.3. PP morphology

While the TEM results allow a clear observation of the PC morphology as described above, differences in the PP morphology as a function of processing are not readily apparent from these microscopy results. Crystalline PP structures are visible in the TEM (Figs. 4 and 8), but specific details about the size of these crystalline domains is presently lacking. Foreign matter present within a molten semicrystalline polymer material is typically the nucleating agent for crystallization. This would suggest that the PC domains might provide a surface to nucleate PP crystal growth. Using this argument for PC acting as nucleating agent for PP crystal growth, it was conjectured that the small PC domains would be located at the epicenter of the crystalline structures within PP phase [19]. However, this was not observed for these nanoblends, as observed in the image of Fig. 4, where a crystalline PP spherulitic structure is present with no PC domain at its center. Rather the PP spherulite crystals appear to be nucleated by another source and then subsequently grow around (and unperturbed by) the polycarbonate domains as illustrated in Figs. 7 and 8. It is remarkable that these results are consistent with the expectation that the nanostructures of the polymer blends are not destroyed by crystallization, which has a much larger thermodynamic driving force but operates at smaller length scales of about 2–7 nm [42].

From the ^{1}H and ^{13}C MAS NMR spectra it is known that both mobile and immobile PP components are present in these samples. It is possible using ^{1}H spin diffusion experiments [43,44] to measure the different PP domain sizes. By utilizing a ^{1}H dipolar-filter that preferentially selects out those protons having a longer spin–spin T_2 relaxation time it is possible to obtain spectra that are dominated by the mobile (or amorphous) PP phase. By measuring the transfer of magnetization back to the immobile (crystalline) PP phase due to ^{1}H spin diffusion, an estimate of the domain size for immobile (crystalline) PP component is obtained.

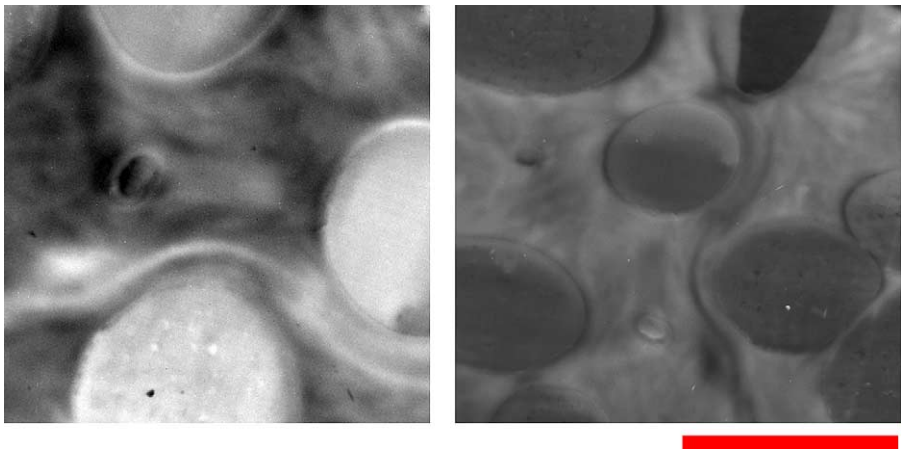

Fig. 7. STEM images of crystal growth around PC dispersions indicating that PP crystal growth occurs around existing PC domains. Both images are of an *m*PP-*g*-PC 80:20 blend. The left image is a TEM bright-field image and the right image is a STEM dark-field image. Scale bar equals 5 μm.

Fig. 9 shows the ^{1}H dipolar-filtered ^{13}C CPMAS NMR spin diffusion experiment for the *m*PP-*g*-PC 90:10 (I-ML) nanoblend. Immediately following the dipolar filter (1 ms) only those ^{13}C resonances associated with mobile (long T_2) protons are visible. These resonances at $\delta = 41.9$, 24.2 and 19.0 ppm correspond to the CH_2, CH and CH_3 carbons of the mobile (amorphous) component of PP, respectively. This result confirms the previous assignment of ^{13}C NMR resonances given in Fig. 2 for pure PP. Note that the aromatic resonances at $\delta = 145.3$, 123.6 and 116.3 ppm arising from the PC component are completely suppressed, along with the crystalline PP resonances at $\delta = 40.0$ and 22.1 and 17.7 ppm. With increased NMR mixing times the exchange of magnetization via ^{1}H–^{1}H spin diffusion allows for the recovery of some of the suppressed resonances. In particular, the immobile (crystalline) PP resonances recover, allowing for a measure of the spin diffusion rate. The recovery of the immobile (crystalline) PP methylene resonance ($\delta =$ 40.0 ppm) is shown in Fig. 10(a). Similar recovery curves for the methane ($\delta = 22.1$ ppm) and methyl ($\delta = 17.7$ ppm) ^{13}C resonance were also obtained, even though the methyl group has significant spectral overlap with the amorphous methyl resonance. For the spin-diffusion mixing times investigated no recovery of the PC aromatic signals was observed due to the large PC domain size.

While these ^{13}C detected ^{1}H–^{1}H NMR spin diffusion experiments are powerful, they are also rather time consuming depending on the number of NMR spin-diffusion mixing times investigated. It is also possible to measure the ^{1}H–^{1}H spin diffusion with direct ^{1}H detection. For this experiment we were able to preferentially select the mobile PP ^{1}H component via a dipolar filter, and then monitor the recovery of the immobile (broad) ^{1}H signal from the PP or the crystalline PC. An example of the recovery of the immobile (crystalline) PP signal as a function of spin-diffusion mixing time is shown in Fig. 10(b). These results are very similar to those obtained in the ^{13}C detected ^{1}H–^{1}H spin diffusion experiments presented above (Fig. 10(a)). Similar ^{1}H spin diffusion curves were obtained for the nanoblend samples A-ML to H-ML (Table 2).

There are a variety of analysis methods that have been employed to determine domain size from NMR spin diffusion data. These methods include simple approximations based on

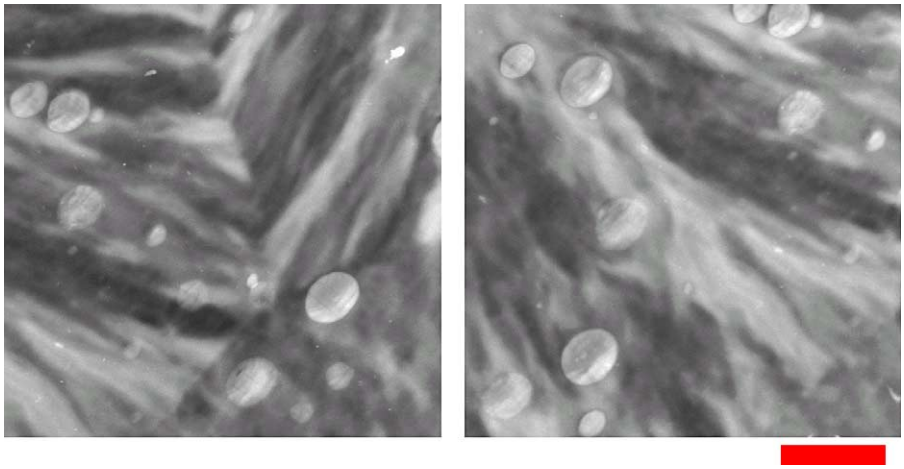

Fig. 8. STEM of *m*PP-*g*-PC 95:05 (PD) at 8500×. This higher magnification further supports the idea that the PC dispersions do not center of the PP growth patterns, and are probably not the point of crystal nucleation. The figure on the left is the boundary of two PP spherulites, where the figure on the right is of the middle of spherulites. Scale bar equals 1.5 μm.

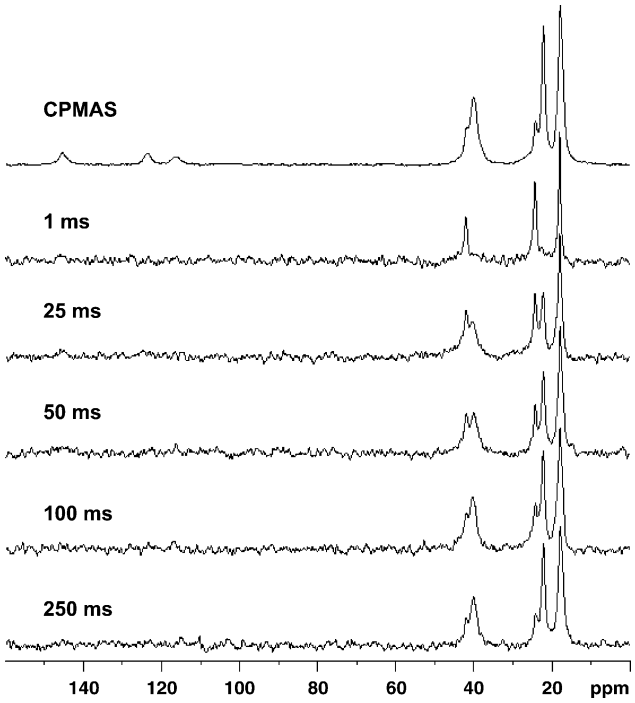

Fig. 9. The ^{13}C detected ^{1}H spin diffusion NMR spectra of the *m*PP-*g*-PC 90:10 blend at a measurement temperature of 75 °C as a function of NMR mixing time.

initial rates of magnetization build-up or more complex analytical and numerical solutions of the diffusion equation. The nanoblends investigated here are best described by a three-component mixture and the corresponding interfaces, i.e. PC, immobile (crystalline) PP and mobile (amorphous) PP. From the ^{13}C-detected (Fig. 9) and the ^{1}H-detected (spectra not shown) ^{1}H spin diffusion results, it is readily apparent that there is no recovery of the PC signal for mixing times (τ_m) out to ~250 ms. This is most easily seen by inspecting the aromatic region of the ^{13}C NMR spectra (Fig. 9) $\delta = 145$–115 ppm. This result shows that the fraction of mobile PP component within spin-diffusion contact of the PC component is negligible. It appears that even for this particular blend (I-ML) with a PC domain size of ~200 nm, these types of NMR spin diffusion experiments are still limited by relaxation effects. Based on the detailed discussion below, analysis of these 200 nm PC domain via spin-diffusion would require mixing times nearly 400 times larger than pursued in the present experiment, and would be unsuccessful due to PC T_1 spin–lattice relaxation.

Since the PC component in the nanoblends is not involved in ^{1}H spin diffusion process for short NMR mixing times, the nanoblends can be described by a simple two component model. The average domain size (d) of the immobile (crystalline) PP domain dispersed within the mobile (amorphous) PP matrix can be estimated using: [38,43,45]

$$d = \left(\frac{\rho_{HA}\phi_A + \rho_{HB}\phi_B}{\phi_A\phi_B}\right)\left(\frac{4\varepsilon\phi_A}{\sqrt{\pi}}\right)\left(\frac{\sqrt{D_A D_B}}{\sqrt{D_A}\rho_{HA} + \sqrt{D_B}\rho_{HB}}\right)\sqrt{\tau_m^*} \quad (1)$$

where ρ_{HA}, ρ_{HB} ϕ_A, ϕ_B, D_A and D_B are the proton density, volume fraction, and spin–diffusion coefficient, respectively, of the immobile (A) and mobile (B) PP domains, respectively. The dimensionality of the PP domain is defined by the ε, and $\sqrt{\tau_m^*}$ is the mixing time that corresponds to the intersection of the initial magnetization build-up with the equilibrium magnetization intensity (Fig. 10).

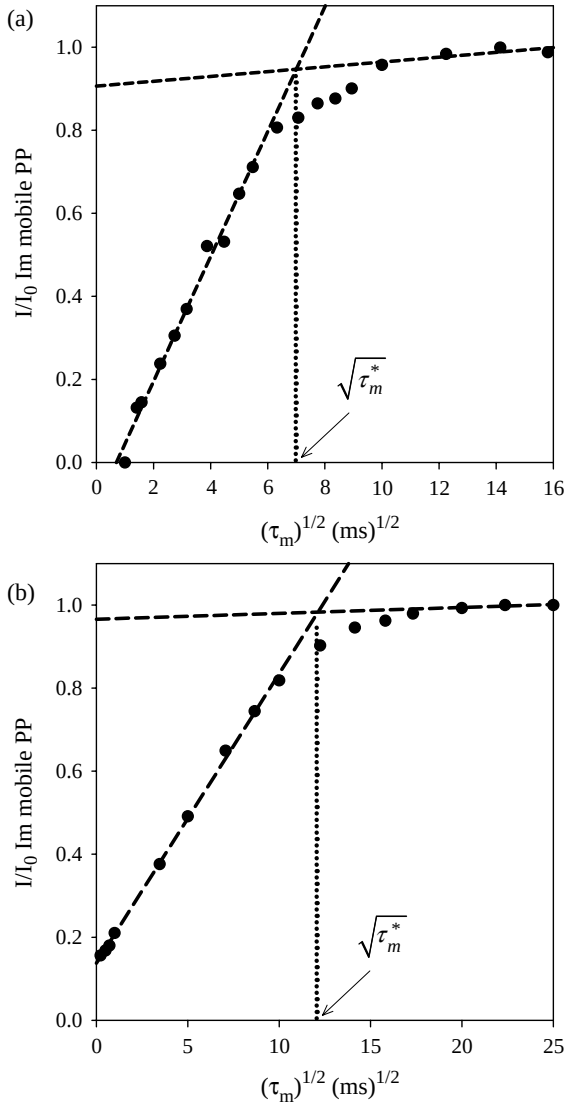

Fig. 10. Spin diffusion recovery curves as a function of the square root of the NMR spin-diffusion mixing time for (a) *m*PP-*g*-PC 90:10 based on the ^{13}C MAS NMR detected spin diffusion experiment (Fig. 9) and (b) for *m*PP-*g*-PC 80:20 from the ^{1}H MAS NMR detected spin diffusion experiment. The equilibrium spin-diffusion mixing time $\sqrt{\tau_m^*}$ which is used in Eq. (1) are denoted.

Using the bulk polypropylene density values of 0.95 g/cm^3 (crystalline phase), 0.85 g/cm^3 (amorphous phase) and 0.91 g/cm^3 (bulk PP) the proton densities of the mobile (amorphous) PP was estimated to be 0.135 g/cm^3 and the immobile (crystalline) PP to be 0.121 g/cm^3. From Table 2, the PP is ~60% crystalline by weight giving molar volume fractions for the mobile and immobile PP phases of 0.323 and 0.676, respectively.

A reliable estimate of the proton spin diffusion coefficient (D), which is proportional to the through-space couplings present within the nanoblend, is also required. In previous investigations, spectral line widths of static ^{1}H NMR spectra have been used to estimate the spin diffusion coefficient, but this can be complicated by spectral overlap of different proton resonances (as in the case of the nanoblends investigated here). There also exist relationships between the effective spin–spin relaxation rate $[(T_2^*)^{-1}]$ and the spin diffusion coefficient in static samples given by Ref. [38]

$$D\left[\left(T_2^*\right)^{-1}\right] = \left(8.2\times10^{-6}\left[T_2^*\right]^{-3/2} + 0.007\right)\ \mathrm{nm^2/ms}, \quad 0 < \left[T_2^*\right]^{-1} < 1000\ \mathrm{Hz} \tag{2}$$

$$D\left[\left(T_2^*\right)^{-1}\right] = \left(4.5\times10^{-5}\left[T_2^*\right]^{-1} + 0.26\right)\ \mathrm{nm^2/ms}, \quad 1000 < \left[T_2^*\right]^{-1} < 3500\ \mathrm{Hz} \tag{3}$$

It should be noted that these relationships were proposed for non-spinning (static) ^{1}H NMR measurements, and their use for ^{1}H MAS NMR based experiments may not be directly applicable. On the other hand is known that both the ^{1}H spin diffusion coefficient and the ^{1}H T_2 relaxation are determined by the dipole–dipole interaction, and that MAS and internal motions will reduce the effectiveness of this coupling. Therefore, as a first approximation we will utilize the relationships in Eqs. (2) and (3) to provide an estimate of D under MAS conditions, but because of this assumption we will denote it as the effective spin diffusion constant. Using Eqs. (2) and (3) the T_2^* of ~5.5 ms for the mobile methane and methylene protons of PP, and ~300 μs T_2^* for the broad immobile protons of PP, estimates $D[(T_2^*)^{-1}]$ of 0.03 and 0.41 nm^2/ms, respectively. The estimate for $D[(T_2^*)^{-1}]$ in the crystalline PP is very close to the 0.56 nm^2/ms previously reported [46]. Also note that since the T_2^* values are both temperature and spinning speed dependent they were determined at 90 °C and a spinning speed of 30 kHz, the same as the ^{1}H detected spin diffusion experiments in Fig. 10(b). The T_2^* was not determined at the slower spinning speed (10 kHz) or the 75 °C used in the ^{13}C detected spin diffusion experiments (Fig. 9), but as a first approximation the high speed spin diffusion coefficients will be used, and is expected to introduce a small error in the determination of the effective spin diffusion coefficient. Regardless of the error introduced in using Eqs. (2) and (3) for estimating an effective spin diffusion constant, the comparison of the relative domain size due to differences in processing between the different blends is still valid.

The $\sqrt{\tau_m^*}$ values for the different nanoblend samples investigated are given in Table 2. Using Eq. (1) the domain sizes are predicted to range from 5 to 16 nm, depending on the dimensionality (ε) of the immobile (crystalline) PP phase, and are listed in Table 2. The initial rate approximation suffers from the difficulty in being able to distinguish domain size effects from dimensionality effects [44]. These predicted domain sizes appear to be consistent with those reported for isotactic PP and interpreted using a polydisperse lamellar model [42]. Additional details about the dimensionality for these nanoblends obtained from either microscopy or small angle diffraction is needed, but presently unavailable. Given this uncertainty, the domain sizes for different dimensionalities are given in Table 2. These immobile (crystalline) PP domain sizes are too small to be the length of the entire crystal/spherulite as the electron microscopy images (Fig. 4) indicate crystalline structures with diameters greater than 20 μm. The probable explanation is that the domain size estimated by NMR represents the lamellar thickness within the crystalline structures similar to that reported by Ryan and co-workers for isotactic PP [42]. This hypothesis is supported by the fact that an amorphous region is thought to be present between crystalline lamella [34]. This explanation is also supported by the idea that lamellar thicknesses for isotactic polypropylene are usually in the range of 1–20 nm [42]. Regardless of the dimensionality or model used, these ^{1}H detected NMR spin diffusion results show that for the 80:20 *m*PP-*g*-PC samples (A-ML through H-ML) the immobile (crystalline) PP domain size is invariant to processing conditions. For the 90:10 nanoblend (Sample I-ML) there is a reduction in the domain size down to ~10 nm ($\varepsilon = 3$). Whether this change in domain size is a result of solely the compositional variation or from the reduced processing temperature (200 °C versus 225 °C, Table 1) will be investigated in future proposed research.

5. Conclusions

A series of different in situ polymerized nanoblends processed under different conditions were investigated to determine structural and morphology variations. These experiments reveal that for these nanoblends the PC phase morphology is highly dependent on the specifics of the sample preparation conditions, in particular the composition and mix temperature. Interestingly, it is possible under specific conditions to produce nanostructured polymer blends with uniform PC ellipsoidal dispersions with average dimensions of 210 nm × 150 nm. Under the synthesis and processing conditions used, the crystalline morphology of the PP phase shows almost no variation with processing conditions of mixing time and processing shear rates or RPM, suggesting an average immobile (crystalline) domain size of ~16 nm. By changing composition and processing temperature the domain size of the immobile (crystalline) PP phase decreases to ~10 nm. The remarkable stability and robustness of the nanosized crystalline PP phase structures of the special polymer blends of this study is ascribed to the fact that they are not destroyed by PC crystallization, which has a much larger thermodynamic driving force but operates at smaller length scales. Further work will focus on correlating the key results of the present study with those obtained from X-ray diffraction, light scattering and rheology experiments.

Acknowledgements

This work was primarily supported by the Chemical and Transport Systems Program of the National Science Foundation under Award Number CTS 0317646. J.U.O. acknowledges the research of his former graduate students and postdocs. We thank Dr Daniel Brunelle of General Electric for providing the macrocylic carbonates and helpful discussions with him improved the quality of this work. T.M.A, B.R.C, and G.P.H acknowledge partial support by the DOE BES program at Sandia. The student intern program (SIP) at Sandia is also acknowledged (D.R.). Sandia is a multiprogram laboratory operated by Sandia Corporation, a Lockheed Martin Company, for the United States Department of energy's National Nuclear Security Administration under Contract DE-AC04-94AL85000.

References

[1] (a) Utracki LA. Polymer alloys and blends. Munich: Hanser; 1990.
(b) Paul DR, Bucknall CB, editors. Polymer blends. New York, NY: Wiley; 2000.
[2] Daly LE. US Patent No. 2,439,202; 1948.
[3] Sundaraj U, Macosko CW, Rolando RJ, Chan HT. Polym Eng Sci 1992; 32:1814–23.
[4] Tucker III CL, Moldenaers P. Ann Rev Fluid Mech 2002;34:177–210 [and references therein].
[5] Van Hamerlrijck E, Van Puyvelde P, Macosko CW, Molenaers P. J Rheol 2005;49:783–98.
[6] Hu G-H, Kadiri I. J Polym Sci, Part B: Polym Phys 1998;36:2153–63.
[7] Ide F, Hasegawa A. J Appl Polym Sci 1974;18(4):963–74.
[8] Baker W, Scott C, Hu G-H, editors. Reactive polymer blending. Munich: Hanser; 2001.
[9] Ryan AJ. Nat Mater 2002;1:8–10.
[10] (a) Guo MM, Brittain WJ. Macromolecules 1998;31:7166–71.
(b) Guo MM, Brittain WJ. Polym Prepr Am Chem Soc, Div Polym Chem 1998;39:385–6.
(c) Guo MM. Polym Prepr Am Chem Soc, Div Polym Chem 1997;38: 884–5.
[11] Cha J, White JL. Polym Eng Sci 2001;41:1227–37.
[12] Kim B, White JL. SPE ANTEC Tech Papers 1995;53:242–9.
[13] (a) Otaigbe JU. Advances in polymer science. vol. 154. Berlin: Springer; 2001 p. 1–86.
(b) Moriarty P. Rep Prog Phys 2001;64:297–381.
[14] Pernot H, Baumert M, Court F, Leibler L. Nat Mater 2002;1:54–8.
[15] Xanthos M. Reactive extrusion. Munich: Hanser; 1992.
[16] (a) Mcgrath JE, editor. Ring-opening polymerization: kinetics, mechanisms, synthesis. Washington, DC: American Chemical Society; 1985.
(b) Ivin KJ, Saegusa T, editors. Ring-opening polymerization, 3. London: Elsevier Applied Science; 1984.
(c) Macosko CW. RIM, fundamentals of reaction injection molding. Munich: Hanser; 1989.
[17] (a) Otaigbe JU. Trends Polym Sci 1997;5(1):1–23.
(b) Otaigbe JU. J Appl Polym Sci 1992;45:1213–21.
[18] Udipi K, Dave RS, Kruse RL, Stebbins LR. ACS Symp Ser 1998;696: 255–66.
[19] Madbouly SA, Rhoades D, Otaigbe JU. SPE-ANTEC Tech Pap 2005;63: 2413–7.
[20] Otaigbe JU. Trends Polym Sci 1997;5:17–23 [and references therein].
[21] Brunelle DJ, Shannon TG. US Patent 4 904 810; 1989.
[22] Evans TL, Berman CB, Carpenter JC, Choi DY, Williams DA. Polym Prepr Am Chem Soc, Div Polym Chem 1989;30(2):573–4.
[23] Stewart KR. Polym Prepr Am Chem Soc, Div Polym Chem 1989;30(2): 575–6.
[24] Brunelle DJ. Trends Polym Sci 1995;3(5):154–8 [and references therein].
[25] Brunelle DJ, et al. Polym Prepr Am Chem Soc, Div Polym Chem 1989; 30(2):569–70.
[26] Brunelle DJ, Shannon TG. Macromolecules 1991;24(11):3035–44 [and references therein].
[27] Brunelle DJ, Shannon TG. Polym Prepr Am Chem Soc, Div Polym Chem 1990;31(1):14–15.
[28] Evans TL, Carpenter JC. Polym Prepr Am Chem Soc, Div Polym Chem 1990;31(1):18–19.
[29] Evans TL, Brunelle DJ, Salem AJ, Stewart KR. Polym Prepr Am Chem Soc, Div Polym Chem 1991;32(2):176–7.
[30] (a) Kambour RP, Nachlis WL, Carbeck JD. Polymer 1994;35(1):209–11.
(b) See alsoNachlis WL. Polymer 1994;35(17):3643–57.
[31] Hu G-H, Cartier H. Macromolecules 1999;32:4713–8.
[32] Teng J, Otaigbe J, Taylor E. Polym Eng Sci 2004;44:648–59.
[33] Velankar S, Zhou H, Macosko CW. In ANTEC: Nashville, TN; 2003.
[34] Gedde UW. Polymer physics. Boston: Kluwer Academic Publishers; 1999.
[35] Bennett AE, Rienstra CM, Auger M, Lakshmi KV, Griffin RG. J Chem Phys 1995;103:6951–8.
[36] Cai WZ, Schmidt-Rohr K, Egger N, Gerharz B, Spiess HW. Polymer 1993;34:267–76.
[37] Mirau PA, Yang S. Chem Mater 2002;14:249–55.
[38] Mellinger F, Wilhelm M, Spiess HW. Macromolecules 1999;32:4686–91.
[39] Gomez MA, Tanaka H, Tonelli AE. Polymer 1987;28:2227–32.
[40] Aoki A, Asakura T. In: Ando I, Asakura T, editors. Polyolefins in solid state NMR of polymers. Studies in physical and theoretical chemistry, vol. 84. New York: Elsevier Science; 1998. p. 415–44 [chapter 11].
[41] Saito S, Moteki Y, Nakagawa M, Horii F, Kitamaru R. Macromolecules 1990;23:3256–60.
[42] Ryan AJ, Stanford JL, Bras W, Nye TMW. Polymer 1997;38:759–68.
[43] Clauss J, Schmidt-Rohr K, Spiess HW. Acta Polym 1993;44:1–17.
[44] VanderHart DL, McFadden GB. Solid State Nucl Magn Reson 1996;7: 45–66.
[45] Schmidt-Rohr K, Spiess HW. Multidimensional solid-state NMR of polymers. San Diego: Academic Press Limited; 1994.
[46] Quijada-Garrido I, Wilhelm M, Spiess HW, Barrales-Rienda JM. Macomol Chem Phys 1998;199:985–95.